THE ASTROPHYSICAL JOURNAL, 556:1010–1016, 2001 August 1

THE INVERSE COMPTON EMISSION SPECTRA IN THE VERY EARLY AFTERGLOWS OF GAMMA-RAY BURSTS

X. Y. WANG, Z. G. DAI, AND T. LU
Department of Astronomy, Nanjing University, 210093 Nanjing, People's Republic of China; xywang@nju.edu.cn, daizigao@public1.ptt.js.cn, tlu@nju.edu.cn
Received 2001 January 12; accepted 2001 April 5

ABSTRACT

We calculate the spectra of inverse Compton (IC) emissions in gamma-ray burst (GRB) shocks produced when relativistic ejecta encounters the external interstellar medium, assuming a broken power-law approximation to the synchrotron seed spectrum. Four IC processes, including the synchrotron self-Compton (SSC) processes in GRB forward and reverse shocks, and two combined-IC processes (i.e., scattering of reverse shock photons on the electrons in forward shocks and forward shock photons on the electrons in reverse shocks), are considered. We find that the SSC emission from reverse shocks dominates over other emission processes in energy bands from tens of MeV to tens of GeV, for a wide range of shock parameters. This mechanism may be responsible for the prompt high-energy gamma rays detected by EGRET. At TeV energy bands, however, the combined-IC emissions and/or the SSC emission from the forward shocks become increasingly dominant for a moderately steep distribution of shocked electrons.

Subject headings: gamma rays: bursts — radiation mechanisms: nonthermal

1. INTRODUCTION

The current standard model for gamma-ray bursts (GRBs) and their afterglows is the fireball shock model (see Piran 1999 for a recent review). It involves a large amount of isotropic equivalent energy release, $E_0 \sim 10^{52}$–10^{54} ergs, within a few seconds and in a small volume with negligible baryonic load, which leads to a fireball that expands ultrarelativistically into the external medium. A substantial fraction of the kinetic energy of the baryons is transferred to a nonthermal population of relativistic electrons through Fermi acceleration in the shock (e.g., Mészáros & Rees 1993). The accelerated electrons cool via synchrotron emission and inverse Compton (IC) scattering in the postshock magnetic fields and produce the radiation observed in GRBs and their afterglows (e.g., Paczyński & Rhoads 1993; Katz 1994b; Sari, Narayan, & Piran 1996; Vietri 1997; Waxman 1997a; Wijers, Rees, & Mészáros 1997). The shock could be either *internal* due to collisions between fireball shells caused by outflow variability (Paczyński & Xu 1994; Rees & Mészáros 1994) or *external* due to the interaction of the fireball with the surrounding interstellar or wind media (Mészáros & Rees 1993; Dai & Lu 1998; Chevalier & Li 1999).

When the relativistic ejecta encounters the external medium, a relativistic *forward* shock expands into the external medium, and a *reverse* shock moves into and heats the fireball ejecta. The shocked ambient and ejecta materials are in pressure balance and separated by a contact discontinuity. The forward shock continuously heats fresh gas and accelerates electrons, producing long-term afterglows through the synchrotron emission (e.g., Waxman 1997a, 1997b; Wijers et al. 1997; Vietri 1997; Wang, Dai, & Lu 2000a, 2000b; Dai & Lu 1999, 2000; Dai, Huang, & Lu 1999; Huang, Dai, & Lu 1998; Huang et al. 2000; Gou et al. 2001). On the other hand, the reverse shock operates only once, and after that emission from the fireball ejecta are suppressed after the reverse shock crosses the ejecta, since then the ejecta expands and cools adiabatically.

When a reverse shock crosses the shell, the shocked shell and the forward shocked external medium carry comparable amounts of energy. However, the typical temperature of the shocked shell electrons is lower since the particle number density is higher. So the typical frequency of the synchrotron radiation from the shocked shell is considerably lower. A strong prompt optical flash (Akerlof et al. 1999) and late-time radio flare behavior (Kulkarni et al. 1999), accompanying GRB 990123, have been attributed to the synchrotron emission process from this reverse shock (Sari & Piran 1999a; Mészáros & Rees 1999).

In a recent paper (Wang, Dai, & Lu 2001; hereafter WDL), we analytically study the high-energy gamma-ray emission from the synchrotron self-Compton (SSC) process in the reverse shocks. The result showed that this emission dominates over the components of the synchrotron and IC emissions from forward shocks at high-energy gamma-ray bands from tens of MeV to tens of GeV. Furthermore, we suggest that this mechanism may explain the observations of the prompt high-energy gamma rays detected by EGRET, such as those from GRB 930131.

In this work, we numerically calculate the SSC radiation components in the forward and reverse shocks. We also consider another two combined-IC processes, i.e., scatterings of reverse shock photons on the forward shocked electrons and forward shock photons on the reversely shocked electrons. For a wide range of shock parameters, the present numerical results confirm our previous suggestions that the SSC emission from reverse shocks is the most important at the energy bands to which EGRET is sensitive.

While IC emissions from afterglow forward shocks (e.g., Sari et al. 1996; Totani 1998a; Waxman 1997b; Panaitescu & Mészáros 1998; Wei & Lu 1998, 2000; Chiang & Dermer 1999; Dermer, Böttcher, & Chiang 2000; Dermer, Chiang, & Mitman 2000; Panaitescu & Kumar 2000) and GRB internal shocks (Papathanassiou & Mészáros 1996; Pilla & Loeb 1998; Panaitescu & Mészáros 2000) have attracted a

lot of investigation, the studies for IC process in reverse shocks and combined-IC scatterings between reverse and forward shocks (i.e., very early afterglows) are still quite preliminary (see, e.g., Mészáros, Rees, & Papathanassiou 1994).

In § 2, we briefly describe the hydrodynamic evolution of a fireball shell. We present in § 3 the synchrotron seed spectra and shocked electron distributions, then perform a numerical calculation of IC emissions in § 4. Finally, we give a summary and discussion in § 5.

2. HYDRODYNAMICS OF A FIREBALL SHELL

Let us consider an ultrarelativistic cold shell with energy E, initial Lorentz factor η, and a width Δ in the observer frame expanding into a cold external interstellar medium (ISM). When the shell sweeps up a large volume of ISM matter, it begins to be decelerated significantly. The interaction between the shell and the ISM matter leads to two shocks: a forward shock propagating into the ISM and a reverse shock moving back into the shell. There are four regions separated by the two shocks and a contact discontinuity: the cold ISM (denoted by the subscript 1), the shocked ISM (subscript 2), the shocked shell material (subscript 3), and the unshocked shell material (subscript 4). From the shock jump conditions and the equalities of pressure and velocity along the contact discontinuity, we can evaluate the Lorentz factor γ, the pressure p, and the number density n in the shocked regions in terms of three variables: n_1, n_4, and η (Blandford & McKee 1976; Sari & Piran 1995).

Sari & Piran (1995) showed that, if the shell is thin—$\Delta < l/2\eta^{8/3}$, where $l \equiv (3E/4\pi n_1 m_p c^2)^{1/3}$ is the Sedov length—the reverse shock is Newtonian (with shell spreading, the reverse shock can be mildly relativistic), which means that the Lorentz factor of the shocked shell material $\bar{\gamma}_3$ is almost unity in the frame of the unshocked shell and $\gamma_3 \sim \eta$. On the other hand, if the shell is thick—$\Delta > l/2\eta^{8/3}$—the reverse shock is relativistic with $\bar{\gamma}_3 \sim \eta/2\gamma_3$, and it then considerably decelerates the shell material (Kobayashi 2000).

After the shell being decelerated, the evolution of the adiabatic forward shock follows the Blandford-McKee solution (Blandford & McKee 1976). For the shocked shell, its dynamic evolution may be complex. Kobayashi & Sari (2000) showed that if the fireball shell has relativistic temperature, the Blandford-McKee solution can be regarded as an adequate description quite early on. But for the case that the reverse shock is only mildly relativistic, the evolution of the shocked shell may deviate the Blandford-McKee solution. This may affect the time evolution of the late-time reverse shock emission but does not affect our computation of the peak-time emission.

3. SYNCHROTRON EMISSION SPECTRA AND ELECTRON DISTRIBUTIONS IN GRB SHOCKS

3.1. *The Synchrotron Seed Spectrum*

The IC emissions depend on both the seed photon spectrum and the shocked electron distribution. We assume the synchrotron seed spectrum to be described by four broken power-law segments as given in Sari et al. (1998). The distributions of newly shocked electrons in both the forward and reverse shocks are assumed to be a power law of index p [$N(\gamma) \propto \gamma^{-p}$], with the minimum Lorentz factor of shocked electrons in the shell rest frame being $\gamma_m = (m_p/m_e)[(p-2)/(p-1)]\xi_e \gamma_{\rm sh}$, where ξ_e is the fraction of thermal energy carried by electrons (Sari et al. 1998). Here for the forward shock $\gamma_{\rm sh} = \gamma_2 = \gamma_3 \equiv \Gamma$, and $\gamma_{\rm sh} = \bar{\gamma}_3$ for the reverse shock. Assuming that ξ_B is the fraction of the thermal energy carried by the magnetic field, the magnetic field strength is $B' = 12G\xi_{B,-2}^{1/2}(\gamma_2/300)n_{1,0}^{1/2}$, where $\xi_{B,-2} = \xi_B/10^{-2}$ and $n_{1,0} = n_1/10^0$. The shocked relativistic electrons cool through synchrotron emission and IC scatterings of the synchrotron photons; thus, the Lorentz factor of the electrons that cool on a timescale equal to the dynamic timescale is given by

$$\gamma_c = \frac{6\pi m_e c(1+z)}{(Y+1)\sigma_{\rm T}\gamma_2(B')^2 t} = \frac{4500}{Y+1}\,\xi_{B,-2}^{-1}\left(\frac{\gamma_2}{300}\right)^{-3} t_1^{-1}\left(\frac{1+z}{2}\right) n_{1,0}^{-1}, \quad (1)$$

where $t_1 = t/10$ s denotes the time in the observer frame, Y is the Compton parameter, z is the redshift of the burst source, and $\sigma_{\rm T}$ is the Thomson scattering cross section. The Compton parameter Y, defined to be the ratio between the IC luminosity of electrons and the synchrotron luminosity, can be expressed as $Y = L_{\rm IC}/L_{\rm syn} = U_{\rm rad}/U_B \sim [-1 + (1 + 4\eta_e \xi_e/\xi_B)^{1/2}]/2$, where $U_{\rm syn}$ and U_B are the energy density of synchrotron radiation and magnetic field, respectively, and η_e represents the fraction of the electron energy that was radiated away (Sari & Esin 2001; Panatescu & Kumar 2000). For fast-cooling electrons, Y is estimated to $(\xi_e/\xi_B)^{1/2}$, and it may be smaller for slow cooling electrons. However, as the two combined-IC processes (i.e., scattering of reverse shock photons on the electrons in forward shocks and forward shock photons on the electrons in reverse shocks) are considered here, the IC cooling of the electrons in both shocks should be dominated by the larger of the two photon fields. Because both shocks have comparable energy, the magnetic field energies in the two shocks are comparable, and therefore Y in two shocks is almost the same and equal to $(\xi_e/\xi_B)^{1/2}$ as long as one shock is in the fast cooling regime.

According to the shell thickness, we divided our discussion into two cases: the thin-shell case and the thick-shell case. The thin-shell case implies that the deceleration timescale $t_{\rm dec}$ (defined as the observer time at which the heated ISM energy is comparable to the initial energy E), i.e.,

$$t_{\rm dec} = \frac{r_{\rm dec}}{2\eta^2 c}(1+z) = 10\left(\frac{1+z}{2}\right) E_{53}^{1/3} n_{1,0}^{-1/3} \eta_{300}^{-8/3} \ {\rm s}, \quad (2)$$

is larger than the shell crossing time (Δ/c), where $E_{53} = E/10^{53}$ ergs and $\eta_{300} = \eta/300$, while the thick shell has $\Delta/c > t_{\rm dec}$. The reverse shock emission peaks at $t_{\rm dec}$ for the thin-shell case and at Δ/c for the thick shell. Our following calculations of the IC spectra correspond to this peak time.

3.1.1. *The Thin-Shell Case*

As described by Sari et al. (1998), the synchrotron radiation from the shocked electrons can be approximated by a broken power-law spectrum with three characteristic break frequencies. One is the self-absorption frequency, ν_a. The other two are the peak frequencies of the emission from the electrons with the characteristic Lorentz factor γ_m and the cooling Lorentz factor γ_c, denoted as ν_m and ν_c, respectively.

As usual, the fraction of thermal energy carried by electrons, ξ_e, and magnetic field, ξ_B, is assumed to be similar in the forward and reverse shock. At the peak time $t_{\rm dec}$ of the reverse shock emission, the break frequencies ν_m from the two shocks are, respectively,

$$\nu_m^{\rm rs} = \frac{1}{1+z}\frac{\Gamma(\gamma_m^{\rm rs})^2 eB'}{2\pi m_e c} = 6.4\times 10^{15}\left(\frac{p-2}{p-1}\right)^2\left(\frac{\xi_e}{0.6}\right)^2 \xi_{B,-2}^{1/2}\eta_{300}^2 n_{1,0}^{1/2} \times\left(\frac{2}{1+z}\right)\ {\rm Hz}\ , \quad (3)$$

$$\nu_m^{\rm fs} = \frac{1}{1+z}\frac{\Gamma(\gamma_m^{\rm fs})^2 eB'}{2\pi m_e c} = 5.6\times 10^{20}\left(\frac{p-2}{p-1}\right)^2\left(\frac{\xi_e}{0.6}\right)^2 \xi_{B,-2}^{1/2}\eta_{300}^4 n_{1,0}^{1/2} \times\left(\frac{2}{1+z}\right)\ {\rm Hz}\ . \quad (4)$$

The equipartition values are chosen to be the ones inferred for GRB 970508: $\xi_e = 0.6$ and $\xi_B = 0.01$ (Granot et al. 1999; Wijers & Galama 1999). Similarly, the cooling break frequencies of both shocks are given by

$$\nu_c^{\rm rs} = \nu_c^{\rm fs} = \frac{1}{1+z}\frac{\Gamma(\gamma_c)^2 eB'}{2\pi m_e c} = \frac{10^{17}}{(Y+1)^2}E_{53}^{-1/2}\xi_{B,-2}^{-3/2}n_{1,0}^{-1} \times\left(\frac{t_{\rm dec}}{10\ {\rm s}}\right)^{-1/2}\left(\frac{2}{1+z}\right)^{1/2}\ {\rm Hz}\ . \quad (5)$$

The peak flux of the synchrotron radiation is given by (Wijers & Galama 1999)

$$f_m = \frac{N_e \Gamma P'_{\nu_m}(1+z)}{4\pi D_L^2}\ , \quad (6)$$

where P'_{ν_m} is the peak spectral power and D_L is the luminosity distance of the burst. Note that for the forward shock, N_e is the total number of swept-up ISM electrons, while for the reverse one, N_e is the total number of shocked shell electrons. Then we obtain the peak flux of the two shocks at the time $t_{\rm dec}$:

$$f_m^{\rm rs} = 4.8\left(\frac{1+z}{2}\right)D_{L,28}^{-2}\xi_{B,-2}^{1/2}\eta_{300}^{-1}n_{1,0}^{1/4}E_{53}^{5/4} \times\left(\frac{2}{1+z}\frac{t_{\rm dec}}{10\ {\rm s}}\right)^{-3/4}\ {\rm Jy}\ , \quad (7)$$

$$f_m^{\rm fs} = 26\left(\frac{1+z}{2}\right)D_{L,28}^{-2}\xi_{B,-2}^{1/2}E_{53}n_{1,0}^{1/2}\ {\rm mJy}\ , \quad (8)$$

where $D_{L,28} = D_L/10^{28}$ cm.

Now we derive the synchrotron self-absorption frequency of the reverse shock emission. In the comoving frame of the shocked gas (denoted with a prime), the absorption coefficient $\alpha'_{\nu'}$ scales as $\alpha'_{\nu'}\propto \nu'^{-(p+4)/2}$ for $\nu' > \nu'_p \equiv \min(\nu'_m, \nu'_c)$ and as $\alpha'_{\nu'}\propto \nu'^{-5/3}$ for $\nu' < \nu'_p$. In this frame, the absorption coefficient for $\nu' < \nu'_p$ is given by (Rybicki & Lightman 1979)

$$\alpha'_{\nu'} = \frac{\sqrt{3}e^3}{8\pi m_e}\left(\frac{3e}{2\pi m_e^3 c^5}\right)^{p/2}(m_e c^2)^{p-1}KB'^{(p+2)/2}\Gamma \times\left(\frac{3p+2}{12}\right)\Gamma\left(\frac{3p+22}{12}\right)\nu_p'^{-(p+4)/2}\left(\frac{\nu'}{\nu'_p}\right)^{-5/3}\ , \quad (9)$$

where $K = (p-1)n_4(4\bar\gamma_3+3)\gamma_p^{p-1}$, $\gamma_p \equiv \min(\gamma_m, \gamma_c)$, e is the electron charge, and $\Gamma(x)$ is the gamma function. Noting that the shocked shell width in the comoving frame $\Delta r' = r/\eta(4\bar\gamma_3+3)$ and setting

$$\tau(\nu'_a) \equiv \alpha'_{\nu'_a}\Delta r' = 1\ , \quad (10)$$

we get the synchrotron self-absorption frequency $\nu_a^{\rm rs}$ in the observer frame,

$$\nu_a^{\rm rs} = 1.4\times 10^{13}E_{53}^{1/5}\eta_{300}^{8/5}\left(\frac{\xi_e}{0.6}\right)^{-1}\xi_{B,-2}^{1/5}n_{1,0}^{9/10}\left(\frac{2}{1+z}\right)\ {\rm Hz} \quad (11)$$

for $p = 2.5$. Similarly, one can obtain the synchrotron self-absorption frequency of the forward shock emission,

$$\nu_a^{\rm fs} = 2.2\times 10^{11}E_{53}^{7/10}\xi_{B,-2}^{6/5}n_{1,0}^{11/10} \times\left(\frac{t_{\rm dec}}{10\ {\rm s}}\right)^{-1/2}(Y+1)\left(\frac{2}{1+z}\right)^{1/2}\ {\rm Hz}\ . \quad (12)$$

Please note that because the forward shock always locates in front of the reverse shock, there will be almost no detected reverse shock emission below the self-absorption frequency of the forward shock. Thus, the synchrotron spectrum of the slow-cooling reverse shock is described by

$$f_\nu^{\rm rs} = f_m^{\rm rs}\begin{cases}0 & \nu < \nu_a^{\rm fs}\\ (\nu/\nu_a^{\rm rs})^2(\nu_a^{\rm rs}/\nu_m^{\rm rs})^{1/3} & \nu_a^{\rm fs} < \nu < \nu_a^{\rm rs}\\ (\nu/\nu_m^{\rm rs})^{1/3} & \nu_a^{\rm rs} < \nu < \nu_m^{\rm rs}\\ (\nu/\nu_m^{\rm rs})^{-(p-1)/2} & \nu_m^{\rm rs} < \nu < \nu_c^{\rm rs}\\ (\nu/\nu_c^{\rm rs})^{-p/2}(\nu_m^{\rm rs}/\nu_c^{\rm rs})^{(p-1)/2} & \nu_c^{\rm rs} < \nu\end{cases}\ , \quad (13)$$

while for the forward shock, which is in the fast cooling regime for typical shock parameters,

$$f_\nu^{\rm fs} = f_m^{\rm fs}\begin{cases}(\nu/\nu_a^{\rm fs})^2(\nu_a^{\rm fs}/\nu_c^{\rm fs})^{1/3} & \nu < \nu_a^{\rm fs}\\ (\nu/\nu_c^{\rm fs})^{1/3} & \nu_a^{\rm fs} < \nu < \nu_c^{\rm fs}\\ (\nu/\nu_c^{\rm fs})^{-1/2} & \nu_c^{\rm fs} < \nu < \nu_m^{\rm fs}\\ (\nu/\nu_m^{\rm fs})^{-p/2}(\nu_c^{\rm fs}/\nu_m^{\rm fs})^{1/2} & \nu_m^{\rm fs} < \nu\ .\end{cases} \quad (14)$$

3.1.2. *The Thick-Shell Case*

In a thick-shell case, the reverse shock becomes relativistic before it crosses the entire shell and begins to decelerate the shell material. It crosses a thick shell at $T \sim \Delta/c$, and the peak time of the reverse shock emission is comparable to the GRB duration T. The Lorentz factor of the shocked shell scales with time as (Sari 1997)

$$\gamma_3 = \left(\frac{l}{\Delta}\right)^{3/8}\left(\frac{4ct}{\Delta}\right)^{-1/4}\ ; \quad (15)$$

thus, the Lorentz factor of the reverse shock at this peak time is

$$\bar\gamma_3 = \eta/2\gamma_3 = 2\,\eta_{500}E_{53}^{-1/8}\left(\frac{2}{1+z}\frac{T}{100\ {\rm s}}\right)^{3/8}n_{1,0}^{1/8}\ . \quad (16)$$

The reference values of the comoving width and the initial Lorentz factor of the thick shell have been chosen to be

$\Delta = 3 \times 10^{12}$ cm and $\eta = 500$, respectively. The shock radius at the peak time of the reverse shock emission is

$$r = 2\gamma_3^2 cT/(1+z) = 5 \times 10^{16} E_{53}^{1/4} n_{1,0}^{-1/4} \left(\frac{2}{1+z}\frac{T}{100\ \mathrm{s}}\right)^{1/4} \mathrm{cm}\ . \quad (17)$$

Using the expressions of γ_m, γ_c, Y parameter, and equation (7), we obtain the break frequencies and peak flux of the reverse shock synchrotron spectrum:

$$\nu_m^{\mathrm{rs}} = 1.8 \times 10^{16} \left(\frac{p-2}{p-1}\right)^2 \left(\frac{\xi_e}{0.6}\right)^2 \times \xi_{B,-2}^{1/2} \eta_{500}^2 n_{1,0}^{1/2} \left(\frac{2}{1+z}\right) \mathrm{Hz}\ , \quad (18)$$

$$\nu_c^{\mathrm{rs}} = \frac{7.6 \times 10^{15}}{(Y+1)^2} \xi_{B,-2}^{-3/2} E_{53}^{-1/2} n_{1,0}^{-1} \times \left(\frac{T}{100\ \mathrm{s}}\right)^{-1/2} \left(\frac{2}{1+z}\right)^{1/2} \mathrm{Hz}\ , \quad (19)$$

$$f_m^{\mathrm{rs}} = 0.3 \left(\frac{1+z}{2}\right) D_{L,28}^{-2} \xi_{B,-2}^{1/2} \eta_{500}^{-1} n_{1,0}^{1/4} E_{53}^{5/4} \times \left(\frac{2}{1+z}\frac{T}{100\ \mathrm{s}}\right)^{-3/4} \mathrm{Jy}\ . \quad (20)$$

Noting that the shocked shell width in the comoving frame $\Delta r' = \Delta\gamma_2/(4\bar{\gamma}_3 + 3)$ and the number density $n_3 = (4\bar{\gamma}_3 + 3)E/(4\pi m_p c^2 \eta\gamma_2 \Delta r^2)$, we can also obtain the self-absorption break frequency ν_a using equation (10) for the thick-shell case. Since for a thick shell, the reverse shock is generally in the fast cooling regime, the synchrotron spectrum is described in a way similar to equation (14).

3.2. *Electron Distribution in Shocked Material*

The electron distribution $N(\gamma)$ in shocked shell or shocked external medium is determined by the initial shocked electron distribution $N_i(\gamma)$, by an electron cooling effect through synchrotron and IC radiation, and possibly by the self-absorption of the synchrotron photons. If the newly shocked electrons with typical Lorentz factor γ_m cools faster than the shock dynamics timescale, the resulting electron distribution takes the form

$$N(\gamma) \propto \begin{cases} \gamma^{-2} & \text{if} \quad \gamma_c < \gamma < \gamma_m \\ \gamma^{-p-1} & \text{if} \quad \gamma_m < \gamma < \gamma_{\max}\ , \end{cases} \quad (21)$$

where $\gamma_{\max}$ is the maximum Lorentz factor of shocked electron, which is determined by equating the electron acceleration timescale with the synchrotron cooling timescale (e.g., Mészáros, Laguna, & Rees 1993); i.e., $\gamma_{\max} = 10^8 B'^{-1/2}$. In the opposite case, most electrons have a random Lorentz factor γ_m, and the electron distribution is

$$N(\gamma) \propto \begin{cases} \gamma^{-p} & \text{if} \quad \gamma_m < \gamma < \gamma_c \\ \gamma^{-p-1} & \text{if} \quad \gamma_c < \gamma < \gamma_{\max}\ . \end{cases} \quad (22)$$

4. IC EMISSIONS FROM VERY EARLY EXTERNAL SHOCKS

After having obtained the seed photon spectrum and the electron distribution, we can now compute the upscattering emissions of the synchrotron radiations by relativistic electrons in the very early external shocks. We consider only the first-order IC and neglect higher order IC processes, because a once-scattered typical photon by a typical electron with γ_e has energy on the order of $(h\nu)_{\mathrm{com}} \gamma_e^3 \gtrsim m_e c^2$ in the rest frame of the second scattering electron. Then we can no longer use the Thomson limit to the scattering cross section, and the energy gained of the scattered photon in each successive scattering will be reduced owing to electron recoil and to the necessity of using Klein-Nishina scattering cross section (Sari & Esin 2001).

For single scattering, the IC volume emissivity in the comoving frame for a distribution $N(\gamma)$ of scattering electrons is given by (Rybicki & Lightman 1979; Sari & Esin 2001)

$$j'^{\mathrm{IC}}_{\nu'} = 3\sigma_{\mathrm{T}} \int_{\gamma_{\min}}^{\gamma_{\max}} d\gamma N(\gamma) \int_0^1 dx g(x) \bar{f}'_{\nu' s}(x)\ , \quad (23)$$

where $x \equiv \nu'/4\gamma^2\nu'_s$, $\bar{f}'_{\nu' s}$ is the incident-specific flux at the shock front in the comoving frame, and $g(x) = 1 + x + 2x\ln(x) - 2x^2$ reflects the angular dependence of the scattering cross section for $\gamma_e \gg 1$ (Blumenthal & Gould 1970). Noting that $f'^{\mathrm{IC}}_{\nu'} = j'^{\mathrm{IC}}_{\nu'} 4\pi r^2 \Delta r'/4\pi D^2$ and the synchrotron flux $f'_{\nu'} = \bar{f}'_{\nu' s} 4\pi r^2/4\pi D^2$, where $\Delta r'$ is the comoving width of the shocked shell or ISM medium and D is source distance, we obtain the IC flux in the observer frame

$$f_\nu^{\mathrm{IC}} = 3\Delta r' \sigma_{\mathrm{T}} \int_{\gamma_{\min}}^{\gamma_{\max}} d\gamma N(\gamma) \int_0^1 dx g(x) f_\nu(x) \quad (24)$$

by transforming equation (23) into the observer frame.

Apart from the SSC scattering processes in the reverse and forward shocks, another two combined-IC scattering processes are also present. Because approximately one-half of the photons raised in one shock region will diffuse into another shock region from the point of view of the comoving frame, the IC flux equation (24) for the combined-IC scatterings should be divided by a factor of 2. Although the scattered photons move isotropically in the comoving frame, the beaming effect makes these photons moving along the direction to the observer.

Our main calculation results are as follows:

1. The IC spectral flux from a relativistic thin shell expanding into an ISM at the deceleration time are shown in Figure 1. Typical shock parameters are used: $E = 10^{53}$ ergs, $\xi_e = 0.6$, $\xi_B = 0.01$, $p = 2.5$, and $n_1 = 1$. Four IC spectra are displayed in the figure, including two SSC spectra from the reverse shock (*solid curve*) and forward shock (*dotted curve*), respectively, scatterings of the reverse shock photons on the forward shocked electrons (*dash-dotted curve*), and the forward shock photons on the reversely shocked electrons (*dashed curve*). From Figure 1, it can be clearly seen that the SSC from the reverse shock dominates over the other three IC components at gamma-ray bands less than a few tens of GeV with a peak around a few MeV. At $\epsilon \sim 10$–100 MeV, the SSC component of the reverse shock exceeds other IC components by about 2 orders of magnitude. Although the peak location of SSC emission strongly depends on this unknown parameter xi_e, this emission dominates over other IC emissions for a wide range of shock parameters.

2. In Figure 2, we present the energy spectra (νf_ν^{IC}) of the IC emissions with various shock parameters for the thin-shell case. We find the following:

a) For a wide range of shock parameters, the SSC component from reverse shocks is the most important at energy bands from tens of MeV to tens of GeV, to which

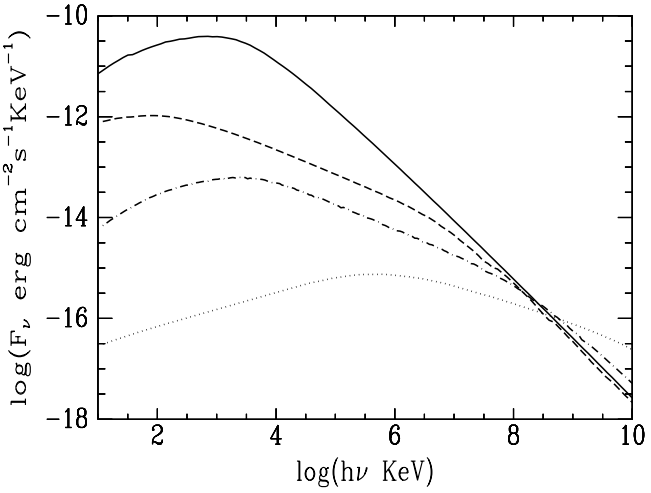

FIG. 1.—Spectra of the IC emissions at the reverse shock peak time for typical shock parameters: $E = 10^{53}$ ergs, $\xi_e = 0.6$, $\xi_B = 0.01$, $p = 2.5$, and an ISM external medium with $n_1 = 1$. The solid and dotted curves represent the SSC emissions from the reverse shock and forward shock, respectively. Also plotted are the IC emissions of scatterings of reverse shock photons on the forward shock electrons (*dash-dotted curve*) and forward shock photons on the reversely shocked electrons (*dashed curve*).

EGRET is sensitive. It dominates over both other IC and the synchrotron emission components.

b) The SSC spectra from reverse shocks above the turnover ($\nu > \nu_p^{IC}$) are logarithmically more flattening than that of the seed synchrotron spectrum and varying continuously. For small values of p, we even find that the IC energy output peak well above min ($\nu_c^{rs,IC}$, $\nu_m^{rs,IC}$), which is the peak emission frequency for the approximate power-law IC spectrum. A similar result was reached by Sari & Esin (2001) for the SSC of afterglow emission. Moreover, for small value of p (e.g., $p = 2.2$), the SSC emission from the reverse shock dominates over the synchrotron and IC processes even in the TeV energy bands (see Fig. 2*d*).

c) Figure 2 also suggests that strong TeV emission should also be emitted from the two combined-IC and forward shock SSC processes for most GRBs. For a moderate steep distribution of the shocked electrons (e.g., $p = 2.5$), the combined-IC and/or forward shock SSC become increasingly dominated at TeV bands. However, it would only be detected from nearby, low-redshift bursts for which the attenuation owing to intergalactic infrared emission is small.

3. EGRET has detected prompt emission above 30 MeV from several bright GRBs triggered by BATSE (Catelli, Dingus, & Schneid 1998), among which GeV photons have been detected from GRB 930131 (Sommer et al. 1994; Ryan et al. 1994) and GRB 940217 (Hurley et al. 1994). GRB 940217 even exhibits delayed GeV emission 90 minutes after the trigger. Several models have been proposed to explain the delayed and prompt GeV emissions. For example, Mészáros & Rees (1994) proposed that the impact of a relativistic wind from the

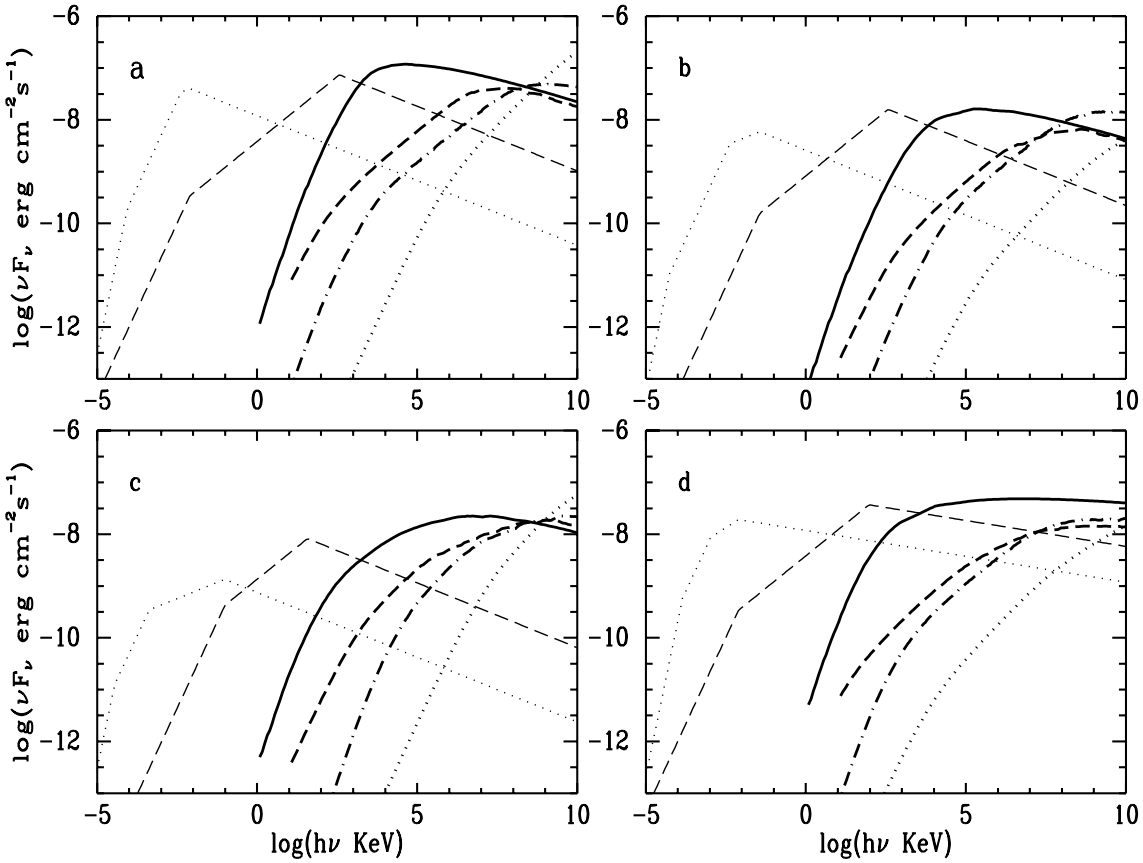

FIG. 2.—Energy spectra of synchrotron and IC emissions at the reverse shock peak time for the ISM circumburst environment case with various shock parameters: (*a*) $E = 10^{53}$ ergs, $\xi_e = 0.6$, $\xi_B = 0.01$, $p = 2.5$, and $n_1 = 1$; (*b*) $E = 10^{52}$ ergs, $\xi_e = 0.6$, $\xi_B = 0.01$, $p = 2.5$, and $n_1 = 1$; (*c*) $E = 10^{53}$ ergs, $\xi_e = 0.6$, $\xi_B = 10^{-4}$, $p = 2.5$, and $n_1 = 1$; (*d*) $E = 10^{53}$ ergs, $\xi_e = 0.6$, $\xi_B = 0.01$, $p = 2.2$, and $n_1 = 1$. The thin dash-dotted and dashed curves represent the synchrotron spectra of the reverse shock and forward shock, respectively. The four IC spectra are shown by the curves in the same way as in Fig. 1.

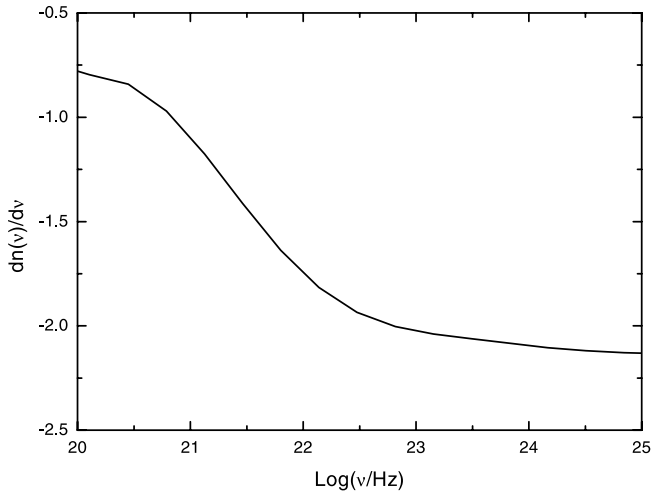

FIG. 3.—High-energy gamma-ray photon spectrum index α of the SSC emission from the reverse shock with shock parameters as used in Fig. 1.

central engine on the external matter may cause the delayed GeV emission; Katz (1994a) suggested that the impact of the fireball on a dense clouds could produce high-energy gamma-ray emission via π^0 decay process; Vietri (1997) and Totani (1998a, 1998b) suggested that the synchrotron radiation of the protons may be responsible for the GeV emissions, etc. In a recent paper (WDL), we have suggested that the SSC emission from the reverse shock could explain both the flux level and the spectrum of the high-energy gamma rays detected by EGRET. We compute here the slope of the photon spectrum at high-energy bands and plot it in Figure 3. We can see that at energy bands from tens of MeV to tens of GeV, the photon spectrum index α [the photon number $dn(h\nu)/d\nu \propto \nu^{\alpha}$] ranges from 1.7 to 2.15, which is consistent with the observed high-energy gamma-ray photon spectrum by EGRET from some bright GRBs (e.g., Sommer et al. 1994).

4. Then we investigate the SSC emission from the reverse shock of a thick shell. We compute the time-integrated SSC energy spectrum for a thick shell with typical parameters as $\Delta = 3 \times 10^{12}$, $E = 10^{53}$ ergs, $p = 2.5$, and $n_1 = 1$, but with different values of the initial Lorentz factor η: $\eta = 300$ (*dash-dotted curve*), $\eta = 500$ (*dashed curve*), and $\eta = 1000$ (*dotted curve*). They are plotted in Figure 4 in comparison with the thin-shell case (*solid curve*). As η increases, the peak frequency of the time-integrated SSC energy spectrum increases accordingly. The peak frequency of SSC emission of the thick shell is not far from that of the thin-shell case with the same η and typical shock parameters, although the reverse shock of the thick shell is relativistic. This is because this IC emission peaks at $\nu_c^{\rm rs,\,IC}$ (this reverse shock is in the fast cooling regime), which is close to $\nu_m^{\rm rs,\,IC}$ for the thin shell. Figure 4 also shows that the peak flux is much lower than the thin-shell case. The reason is that at the peak time of the reverse shock emission, the shell has traveled to a larger distance, resulting in a lower electron scattering optical depth in the shell.

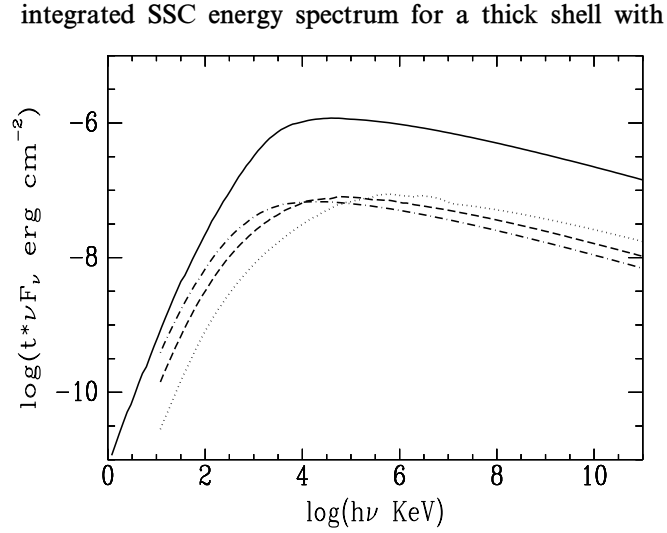

FIG. 4.—Comparison of the time-integrated energy spectrum between the thin-shell case (*solid curve*) with shock parameters as used in Fig. 1 and the thick-shell case with the same shock parameters $E = 10^{53}$ ergs, $\Delta = 3 \times 10^{12}$ cm, $p = 2.5$, and $n_1 = 1$ but with different values of η: $\eta = 300$ (*dash-dotted curve*), $\eta = 500$ (*dashed curve*), and $\eta = 1000$ (*dotted curve*).

5. SUMMARY AND DISCUSSION

The fireball model for GRBs involving an ultrarelativistic fireball ejecta expanding into an external medium has two successful predictions: one is the afterglow emission from the synchrotron process in the forward shock region (Katz 1994b; Mészáros & Rees 1997), and another is the prediction of bright optical emission when a reverse shock is present (Sari & Piran 1999b). Subsequent observations of multiwavelength afterglows (e.g., Wijers, Rees, & Mészáros 1997) and a bright optical flash (Akerlof et al. 1999) gave basic confirmation of this model. In this paper, we calculate the SSC and combined-IC emissions from these two shock regions at very early phases. For a wide range of shock parameters, the SSC emission from the reverse shock dominates over the synchrotron and other IC emissions at energy bands from tens of MeV to tens of GeV, while the combined-IC and/or the forward shock SSC emissions become increasingly dominant at TeV energy bands.

We further compute the photon spectrum index α [viz., $dn(h\nu)/d\nu \propto \nu^{-\alpha}$] of the reverse shock SSC emission, which is $\alpha \sim 2.0$ for typical shock parameters at energy bands to which EGRET is sensitive. On the basis of this and the SSC spectral flux level, we suggest that this process can provide a plausible explanation for the prompt high-energy gamma rays detected from some bright bursts, such as those from GRB 930131, GRB 910503, and GRB 940217, etc. In WDL, we also derived the decaying light curves of SSC emission after the reverse shock peak time and found that it decays quite rapidly, regardless of whether the observed band locates above or below the cooling break frequency of the IC component. The planned Gamma-Ray Large Area Space Telescope mission will have a larger effective area and field of view than EGRET and so will likely be able to monitor the time evolution of the high-energy gamma-ray flux.

At TeV energy bands, the combined-IC emissions and the SSC emission from the forward shock become dominant over the SSC from the reverse shock for intermediate values of p (e.g., $p = 2.5$). Nevertheless, for small values of p, the SSC from the reverse shock still dominates even in TeV energy bands. Recently, the Milagro group reported evidence for TeV emission from GRB 970417a, one of the 54 BATSE GRBs in the field of view of their detector, Milag-

rito (Atkins et al. 2000). An excess of gamma rays above background is seen during the durations of this burst, and the chance probability for detecting such an excess is estimated to be less than 1.5×10^{-3}. Totani (2000) suggested that proton-synchrotron model of GRBs provides a possible explanation for these observational results. Our calculation is also consistent with detection of TeV emission from GRBs that are near enough to avoid serious attenuation owing to intergalactic infrared radiation field.

Two currently popular models for GRBs are the mergers of compact objects (neutron stars or black holes) and the cataclysmic collapse of massive stars. In the former model, compact objects are expected to have significant spatial velocities so that their mergers would take place at many kiloparsecs outside their birthplaces. Thus, GRBs produced by this model would occur in the ISM with density $n \sim 1$ cm^{-3}. However, if a collapsing massive star (Woosley 1993; Paczyński 1998) is the origin of the GRBs, the circumburst medium is the wind ejected by the star prior to its collapse, whose density decreases outward. In the wind circumburst medium case, the external medium density is much higher than the ISM case at the deceleration length scale, and the magnetic field is much higher accordingly. Therefore, from equation (2), we know that most of the shocked electrons cool to be sub- or transrelativistic ones ($\gamma_c - 1 \lesssim 1$) on the deceleration time $t_{\rm dec}$ (also see eq. [14] in Dai & Lu 2001). With such low values of γ_c, the self-absorbed cyclo-synchrotron radiation and multiple Compton scatterings of these cooled electrons may construct the low-energy part of the resulting spectrum. At the high-frequency part, the spectrum is similar to the fast-cooling spectrum of relativistic electrons; i.e., the spectrum is still in the form of $f_\nu \propto \nu^{-1/2}$ extending up to ν_m and then $f_\nu \propto \nu^{-p}$ upward, produced by the cooling of newly shocked electrons. The resulting IC spectra in this case is therefore much more complicated. Also, we estimate that the IC spectra flux at GeV to TeV bands may be as high as that of the ISM case.

We wish to thank the anonymous referee for his/her constructive and careful comments that enabled us to improve the manuscript. X. Y. W. also thanks D. M. Wei and Z. Li for valuable discussions. This work was supported by the National Natural Science Foundation of China under grants 19973003 and 19825109, and the National 973 project.

REFERENCES

Akerlof, C., et al. 1999, Nature, 398, 400
Atkins, R., et al. 2000, ApJ, 533, L119
Blandford, R. D., & McKee, C. F. 1976, Phys. Fluids, 19, 1130
Blumenthal, G. R., & Gould, R. J. 1970, Rev. Mod. Phys., 42, 237
Catelli, J. R., Dingus, B. L., & Schneid, E. J. 1998, in AIP Conf. Proc. 428, Fourth Huntsville Symp. on Gamma-Ray Bursts, ed. C. A. Meegan, R. D. Preece, & T. M. Koshut (New York: AIP), 309
Chevalier, R. A., & Li, Z. Y. 1999, ApJ, 520, L29
Chiang, J., & Dermer, C. D. 1999, ApJ, 512, 699
Dai, Z. G., Huang, Y. F., & Lu, T. 1999, ApJ, 520, 634
Dai, Z. G., & Lu, T. 1998, MNRAS, 298, 87
———. 1999, ApJ, 519, L155
———. 2000, ApJ, 537, 803
———. 2001, ApJ, 551, 249
Dermer, C. D., Böttcher, M., & Chiang, J. 2000a, ApJ, 537, 255
Dermer, C. D., Chiang, J., & Mitman, K. E. 2000b, ApJ, 537, 785
Gou, L. J., Dai, Z. G., Huang, Y. F., & Lu, T. 2001, A&A, 368, 464
Granot, J., Piran, T., & Sari, R. 1999, ApJ, 527, 236
Huang, Y. F., Dai, Z. G., & Lu, T. 1998, A&A, 336, L69
Huang, Y. F., Gou, L. J., Dai, Z. G., & Lu, T. 2000, ApJ, 543, 90
Hurley, K., et al. 1994, Nature, 372, 652
Katz, J. I. 1994a, ApJ, 432, L27
———. 1994b, ApJ, 422, 248
Kobayashi, S. 2000, ApJ, 545, 807
Kobayashi, S., & Sari, R. 2000, ApJ, 542, 819
Kulkarni, S. R., et al. 1999, ApJ, 522, L97
Mészáros, P., Laguna, P., & Rees, M. J. 1993, ApJ, 415, 181
Mészáros, P., & Rees, M. J. 1993, ApJ, 405, 278
———. 1994, MNRAS, 269, L41
———. 1997, ApJ, 476, 232
———. 1999, MNRAS, 306, L39
Mészáros, P., Rees, M. J., & Papathanassiou, H. 1994, ApJ, 432, 181
Paczyński, B. 1998, ApJ, 494, L45
Paczyński, B., & Rhoads, J. 1993, ApJ, 418, L5
Paczyński, B., & Xu, G. 1994, ApJ, 427, 708
Panaitescu, A., & Kumar, P. 2000, ApJ, 543, 66
Panaitescu, A., & Mészáros, P. 1998, ApJ, 501, 772
———. 2000, ApJ, 544, L17
Papathanassiou, H., & Mészáros, P. 1996, ApJ, 471, L91
Pilla, R., & Loeb, A. 1998, ApJ, 494, L167
Piran, T. 1999, Phys. Rep., 314, 575
Rees, M. J., & Mészáros, P. 1994, ApJ, 430, L93
Ryan, J., et al. 1994, ApJ, 422, L67
Rybicki, G. B., & Lightman, A. P. 1979, Radiative Processes in Astrophysics (New York: Wiley Interscience)
Sari, R. 1997, ApJ, 489, L37
Sari, R., & Esin, A. A. 2001, ApJ, 548, 787
Sari, R., Narayan, R., & Piran, T. 1996, ApJ, 473, 204
Sari, R., & Piran, T. 1995, ApJ, 455, L143
———. 1999a, ApJ, 517, L109
———. 1999b, ApJ, 520, 641
Sari, R., Piran, T., & Narayan, R. 1998, ApJ, 497, L17
Sommer, M., et al. 1994, ApJ, 422, L63
Totani, T. 1998a, ApJ, 502, L13
———. 1998b, ApJ, 509, L81
———. 2000, ApJ, 536, L23
Vietri, M. 1997, ApJ, 478, L9
Wang, X. Y., Dai, Z. G., & Lu, T. 2000a, MNRAS, 319, 1159
———. 2000b, MNRAS, 317, 170
———. 2001, ApJ, 546, L33 (WDL)
Waxman, E. 1997a, ApJ, 485, L5
———. 1997b, ApJ, 489, L33
Wei, D. M., & Lu, T. 1998, ApJ, 505, 252
———. 2000, A&A, 360, L13
Wijers, R. A. M. J., & Galama, T. J. 1999, ApJ, 523, 177
Wijers, R. A. M. J., Rees, M. J., & Mészáros, P. 1997, MNRAS, 288, L51
Woosley, S. E. 1993, ApJ, 405, 273